processes

MDPI

Article

Designing a Turning Guide Vane Using CFD for an Economizer of a Non-Furnace Boiler

Chaerul Qalbi AM [1] and Joon Ahn [2,*]

[1] Department of Mechanical Engineering, Kalimantan Institute of Technology, Balikpapan 76127, Indonesia; chaerul.qalbi@lecturer.itk.ac.id
[2] School of Mechanical Engineering, Kookmin University, 77 Jeongneung-ro, Seongbuk-gu, Seoul 02707, Republic of Korea
* Correspondence: jahn@kookmin.ac.kr

Abstract: Non-furnace boilers can improve the efficiency of industrial once-through boilers. However, temperature non-uniformity occurs in the economizer connected vertically to the boiler. Heat transfer performance is degraded by temperature non-uniformity. To solve this problem, a corbel was installed on the side wall of the economizer, and a baffle was installed on the transition duct. Consequently, although the thermal efficiency of the boiler was improved, significant temperature non-uniformity was still observed in the area upstream of the economizer. To address this issue, this study designed a turning guide vane (TGV) at the economizer inlet using computational fluid dynamics (CFD). First, CFD was performed for a case without a guide vane and a case with an existing baffle installed. By analyzing the streamlines obtained using CFD, two TGV designs were proposed. In the first design, guide vanes were installed along the desired streamline, and the concept of the existing TGV was followed. In the second design, an attempt was made to minimize the pressure drop by arranging guide vanes at the inlet. Both designs reduced the standard deviation of temperature by more than 30% and improved the volume goodness factor by 25%.

Keywords: non-furnace boiler; economizer; turning guide vane; temperature uniformity; pressure drop

Citation: AM, C.Q.; Ahn, J. Designing a Turning Guide Vane Using CFD for an Economizer of a Non-Furnace Boiler. *Processes* **2023**, *11*, 1617. https://doi.org/10.3390/pr11061617

Academic Editor: Ireneusz Zbicinski

Received: 24 March 2023
Revised: 27 April 2023
Accepted: 23 May 2023
Published: 25 May 2023

1. Introduction

With large-scale damages caused by extreme weather events globally, international efforts to combat climate change continue [1]. To reduce CO_2 emissions, it is essential to increase the efficiency of energy-consuming facilities while actively introducing renewable energy sources [2]. The International Energy Agency estimates that the implementation of energy-efficiency measures in industrial boilers can result in a reduction of approximately nine gigatons of CO_2 emissions by 2040 [3]. Since most industrial boilers are of the fire-tube or water-tube type, it is important to increase their efficiency [4,5].

A non-furnace boiler (Figure 1a), mentioned in this study, is a type of boiler that does not use a conventional furnace or combustion chamber; instead, it employs a short-flame burner, such as a metal fiber burner, and directly heats the water tube bank. Non-furnace boilers are more efficient than traditional furnace boilers, as they often leave a smaller footprint and can be designed to generate steam more quickly and efficiently [6].

To further increase the efficiency of non-furnace boilers, economizers can be used to recover heat from the exhaust gases before they are discharged into the atmosphere. Economizers are essentially heat exchangers that use hot exhaust gases to preheat the feedwater before it enters the boiler. This reduces the amount of fuel needed to heat the water to steam, resulting in lower operating costs and reduced greenhouse gas emissions [7,8].

The performance of a boiler economizer can be affected by the inlet temperature uniformity of the combustion gas. A more uniform temperature distribution leads to better performance of the economizer [9]. Ensuring temperature uniformity of combustion gases

at the economizer inlet within a limited installation space can be challenging because economizers are placed vertically to reduce the footprint of non-furnace boilers [10].

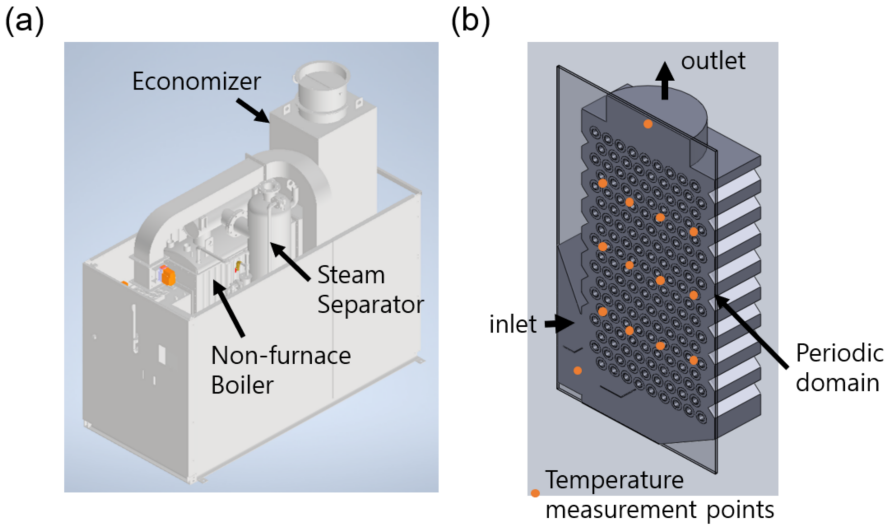

Figure 1. Non-furnace boiler with an economizer; (**a**) 3D shape of the system; (**b**) cross section of the economizer and the computational domain.

As shown in Figures 1b and 2, the economizer of the boiler in this study is a fin-tube heat exchanger. The tube banks are arranged in a staggered array. This setup ensures a higher heat transfer coefficient in the compact heat exchanger than the in-line one [11]; however, as shown in Figure 2a, the flow resistance on the side-wall side is small, so the flow escapes significantly toward this side. To solve this problem, a corbel was installed on the side wall, as shown in Figure 2b [12]. However, side wall corbels cannot prevent the large flow separation that occurs at the economizer inlet.

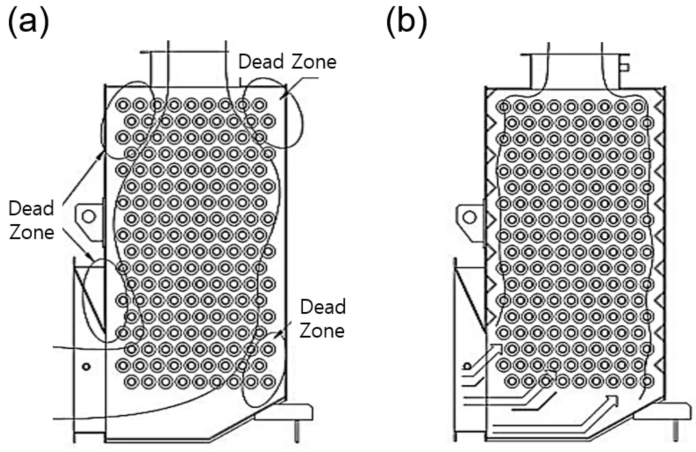

Figure 2. Economizer designs to improve flow uniformity: (**a**) the original design; (**b**) installation of corbels and guide vanes.

Baffles can be installed in the transition duct to help direct the flow of combustion gases and reduce any recirculating flow. Baffles should be designed to create a uniform flow profile and ensure that the combustion gases are distributed evenly across the economizer inlet [13]. Computational fluid dynamics (CFD) results can be used to optimize the design of the transition duct and baffles and help identify any potential hot or cold spots that could affect temperature uniformity [14].

Various types of baffles are installed in the transition duct to increase the temperature uniformity at the economizer inlet. A baffle type that has proven to be effective in increasing temperature uniformity is the swirl vane baffle [15]. The swirling flow helps to distribute the

combustion gases more evenly across the economizer inlet. Another type is the perforated plate baffle [14], where the perforations create a more uniform flow pattern and help to reduce any turbulence or flow disturbances that could affect temperature uniformity. However, both methods cause significant aerodynamic losses [16].

Guide vanes can also help improve velocity uniformity by directing the fluid at an optimal angle and speed. They can be retrofitted to existing equipment, making them a cost-effective way to improve efficiency and reduce operating costs. Guide vanes have been applied to the transition ducts of gas engines and heat recovery steam generators to improve temperature uniformity [17]. As shown in Figure 2b, it was also applied to the economizer in this study. However, the temperature uniformity upstream of the economizer was not satisfactory.

A turning guide vane (TGV) is a type of baffle designed to redirect the flow of combustion gases and create a more uniform flow profile [18]. TGVs have been used at the internal cooling passage of gas turbine blades [19,20]. They can also help improve the temperature uniformity at the economizer inlet. TGVs have been reported to reduce the pressure drop [16] and, thus, improve the overall efficiency of the boiler.

In this study, a TGV was applied to the transition duct connected to the economizer of a non-furnace boiler. The design and configuration of TGVs depend on this specific boiler and economizer configuration and the operating conditions. CFD analysis can be used to optimize the design of TGVs and ensure maximum temperature uniformity and minimum pressure drop [21].

In this study, first, the effect of the existing guide vane (Figure 2b) was reviewed by performing CFD by considering a case without a baffle and the economizer (including the duct) with the installation of the existing guide vane. Next, CFD was performed on the TGV extending from the duct inlet to the tubes to uniformly distribute the flow in the transition duct and compare the output to the results obtained by previous studies. Finally, the temperature uniformity and pressure drop performance were evaluated by performing CFD on the TGV design with a reduced length and rearranged spacing to reduce the pressure loss.

2. Non-Furnace Boilers and Numerical Methods

The boiler simulated in this study was a 3 ton/h class non-furnace boiler. Its operating conditions served as the basis for setting the boundary conditions during the CFD simulation. The overall operating conditions of the boiler are summarized in Table 1. The specifications of the economizer, which was the computational domain of this simulation, are summarized in Table 2. Table 3 shows the natural gas (NG) composition used as the fuel.

Table 1. Operating conditions of the boiler.

Water mass flow	0.838 kg/s
Water inlet temperature	15 °C
Water outlet temperature	79.6 °C
Natural gas fuel mass flow	206 Nm^3/h
Flue gas inlet temperature	254.62 °C
Flue gas outlet temperature	66.6 °C

Table 2. Economizer design data.

Tube outside diameter (D_o)	34 mm
Tube inside diameter (D_i)	28 mm
Transverse spacing (X_t)	66.2 mm
Longitudinal spacing (X_l)	66 mm
Fin length (F_l)	11 mm
Fin thickness (F_t)	0.8 mm
Fin pitch (F_p)	3.2 mm (250 fins per m)
Free-flow area/frontal area	0.512
Total gas-side surface area/total volume	178.91 m^2/m^3

Table 3. Chemical composition of the natural gas fuel.

Chemical Composition	Mole Fraction
Methane (CH_4)	0.88484
Ethane (C_2H_6)	0.09284
Propane (C_3H_8)	0.01405
Butane (C_4H_{10})	0.00812

The mass flow of a combustion gas is calculated using a stoichiometric chemical equation [22]. The mass flow rate corresponds to the excess oxygen (4%) found at the outlet and the composition of NG fuels. For instance, 206 Nm^3/h of fuel is equal to 3187.06 kg/h of flue gas.

Figure 1b shows the three-dimensional shape of an economizer with existing guide vanes installed. The design of the heat exchanger is the staggered finned-tube type. Analyzing this type of heat exchanger required calculating two sides: the water and gas sides. The calculation was done with the assumptions that (1) heat losses to the surroundings were negligible, (2) the flue gas was assumed to have constant properties, (3) no fouling occurred, and a (4) fully developed flow occurred on the water side.

On the water side, the Nusselt number was obtained using the Dittus–Boelter equation according to the Reynolds number [23,24]. The heat transfer coefficient at each tube pass was obtained from the Nusselt number, and the convective boundary conditions were imposed alongside the design bulk temperature, as shown in Figure 2. The design data was obtained through the energy balance in each row mentioned in this section (Figure 3). Table 4 presents the material properties used when calculating the first and last rows on the water side. Through the economizer, the Reynolds number on the water side increased from 3800 to 10,600, and the Prandtl number decreased from 7.86 to 2.51. Since this led to a change in the Nusselt number, i.e., the heat transfer coefficient, the change in the heat transfer coefficient was to be considered in each row. In this simulation, Star-CCM+, a commercial software, was used, and a user-defined function was used to impose the convective boundary conditions based on the location.

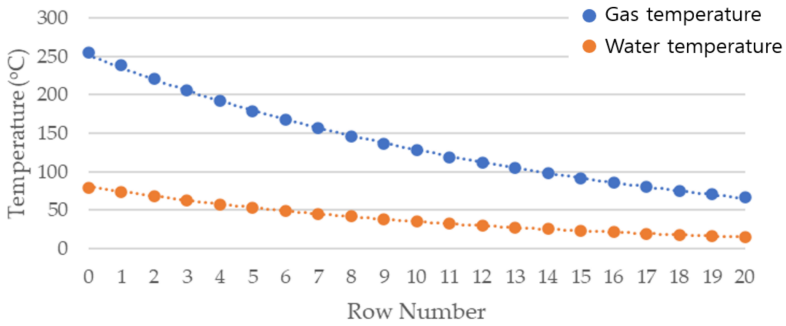

Figure 3. Design temperature data in each row of the economizer.

The gas-side calculation was done with the corresponding j-factor correlation [22]. The appropriateness of the j factor used in this calculation is summarized in Table 5. The Reynolds number on the gas side of the economizer and the geometrical parameters of the fin tube covered in this study are included within the range of experiments performed by [25]. After applying the equation, the fin efficiency [20] was also calculated. In this condition, the tube bank fin efficiency was found to be 0.83. Thus, the overall surface efficiency was calculated. The resulting temperature distribution on the gas side is presented in Figure 2, along with the calculated water side.

In this study, the steady-state Reynolds-averaged Navier–Stokes simulation was performed. The governing equations used in the simulation were the incompressible Navier–Stokes equation and the energy equation. The SIMPLE algorithm was used for pressure-velocity coupling. The advection term was discretized with an upwind scheme of

second-order accuracy. As a turbulence model, a realizable k-epsilon model verified in a similar problem was used [22,26].

Table 4. Properties on the water side.

Row 19	(16.49–15 °C) T_m = 15.745 °C
Density	1000.31 kg/m^3
Kinematic viscosity	1.11 × 10^{-6} m^2/s
Specific heat	4178.83 J/kgK
Prandtl number	7.86
Velocity	0.15118 m/s
Reynolds number	3802.34
Row 1	**(73.86–68.08 °C) T_m = 70.97 °C**
Density	978.48 kg/m^3
Kinematic viscosity	4.08 × 10^{-7} m^2/s
Specific heat	4182.51 J/kgK
Prandtl number	2.51
Velocity	0.15455 m/s
Reynolds number	10,604.33

Table 5. Condition suitability confirmation for the j-factor.

Parameter	Range	Current Value
Flow condition	$1100 \le R_{D_h} \le 18,000$	2,344.61–3,062.29
Outer diameter (D_O)	11.1–40.9 mm	34 mm
Fin pitch (F_P)	246–768 fins/m	250 fins/m
	$0.13 \le \frac{F_p - F_t}{F_l} \le 0.63$	$\frac{F_p - F_t}{F_l} = 0.29$
	$1.01 \le \frac{F_p - F_t}{F_t} \le 7.62$	$\frac{F_p - F_t}{F_t} = 4$
	$0.09 \le \frac{F_l}{D_o} \le 0.69$	$\frac{F_l}{D_o} = 0.32$
	$0.011 \le \frac{F_t}{D_o} \le 0.15$	$\frac{F_t}{D_o} = 0.0235$
	$1.54 \le \frac{X_t}{D_o} \le 8.23$	$\frac{X_t}{D_o} = 1.95$

Figure 4 shows the grid system used for the simulation. The computational domain and grid resolution were determined through two-dimensional preliminary calculations. The computational cells comprised hexahedrons, and $y+$ at the wall was 1. A no-slip boundary condition was imposed on the wall. The maximum expansion ratio of the grid was 1.2. As shown in Figure 1, the 3D computational domain was set to 1 fin pitch in the spanwise direction, and periodic conditions were imposed. About 10 million cells were used for the 3D simulation. The convergence condition was set to 10^{-5}, and it took about 1000 steps to converge.

Experiments were conducted on the boiler shown in Figure 1. A schematic diagram of the experimental setup is shown in Figure 5a. The temperature, pressure, and flow rate of the water and fuel (LNG) supplied to the boiler were measured. In the exhaust gas, the oxygen concentration was measured to evaluate the air ratio and efficiency. To evaluate the combustion characteristics, the concentration of nitrogen oxides (NOx) in the flue gas was measured. Figure 5b shows a picture of the experimental setup.

The boiler was operated at 100% load with an exhaust gas oxygen concentration of 4%. The experiment was then performed. The quality of the produced steam was 99.7%. As shown in Figure 2b, after improving the design of the economizer, the thermal efficiency based on the high heating value of the boiler improved from 91.2% to 92.6%. The NOx concentration in the exhaust gas was about 10 ppm, and there was little difference according to the economizer design change.

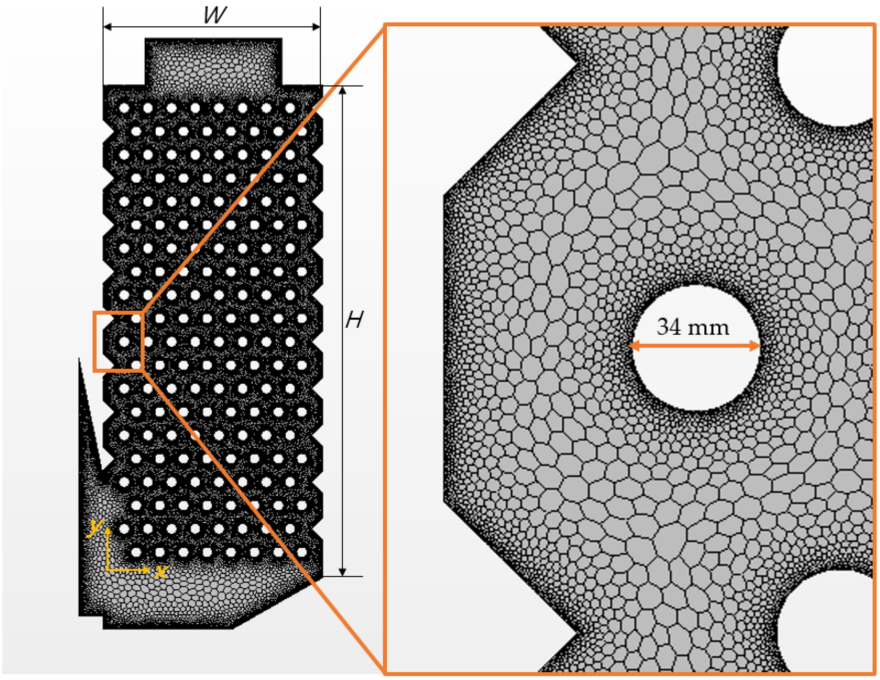

Figure 4. Grid and coordinate system.

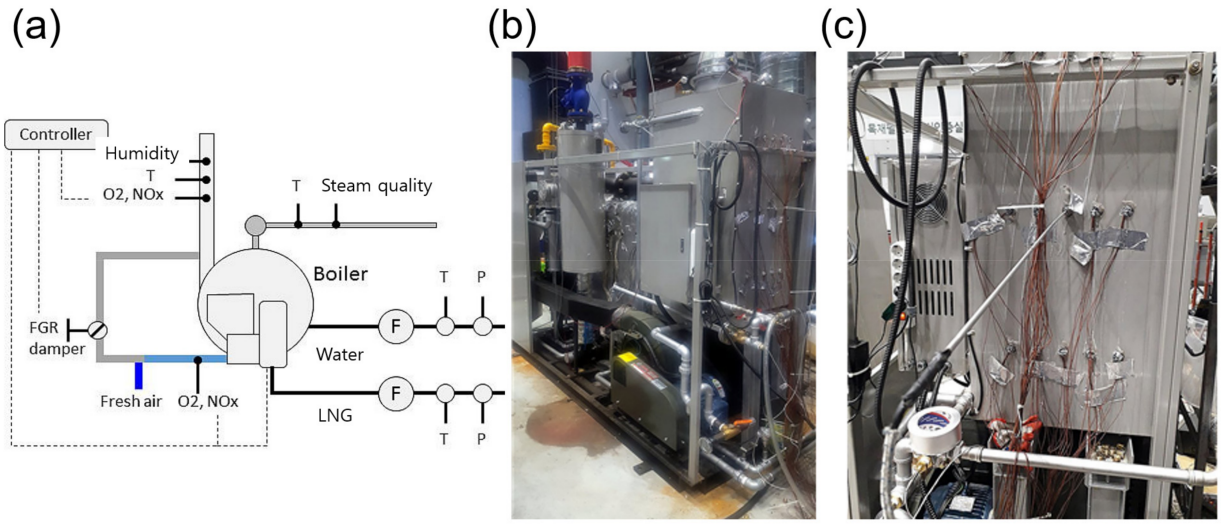

Figure 5. Experimental setup: (**a**) schematic diagram; (**b**) photograph of the non-furnace boiler; (**c**) economizer with temperature sensors.

For the CFD validation, the temperature distribution inside the economizer was also measured. A picture of the economizer and the measuring device is presented in Figure 5c. The temperature distribution was measured in three streamwise locations (rows 5, 10, and 15) inside the economizer. To observe the temperature uniformity, the temperature was measured at four points in the corresponding streamwise position, as shown in Figure 1b. Additionally, the temperature was measured at the inlet and outlet of the economizer. A K-type thermocouple was used for the measurements. The accuracy of the thermocouple used for the measurements was $\pm$ 0.5 °C.

3. Results

Figure 6 compares the CFD data with the experimental and design data for code validation. The design data was obtained through the energy balance in each row mentioned in the previous section (Figure 3). The three pieces of data agreed well with each other.

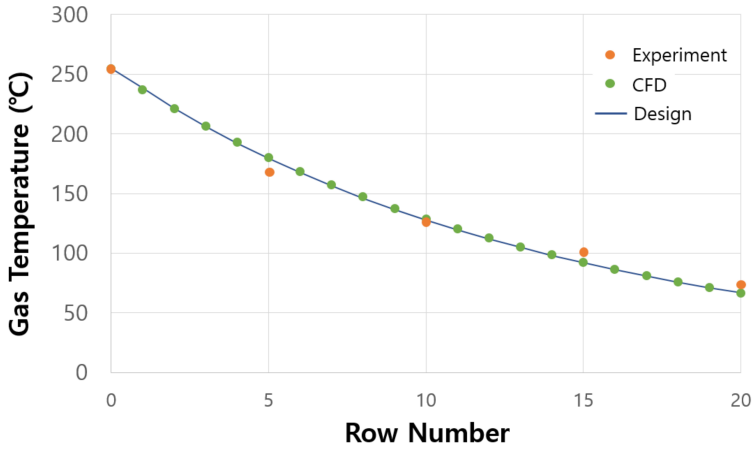

Figure 6. Temperature drop in the direction of gas flow in the economizer.

Figure 7 shows the flow field inside the economizer with the existing baffle installed. First, the problems of the existing baffle were identified by analyzing the streamlines obtained through CFD in Figure 5. By evaluating the design, it was found that even with the baffle, the tube bank could not achieve the preferred gas stream flow. This is because the inlet design allowed the flow to proceed in two directions (horizontal and vertical) to the tube bank.

The follow-up approach was to add a full baffle so that the tube bank received stream flow in only one direction. However, this setup required the baffle because it produced a dead zone as well. To solve this problem, two different TGVs were proposed, as follows.

First, to improve the inactive heat transfer in the upstream tube bank near the duct's wall, it was extended to the position of the upstream tube. A TGV was designed in the open area of the economizer inlet. TGV 1 (Figure 8a) follows the geometry commonly seen in previous studies [18,19]. It was designed in such a way that the mass flow was divided in proportion to the cross-sectional area and continued from the inlet to the outlet.

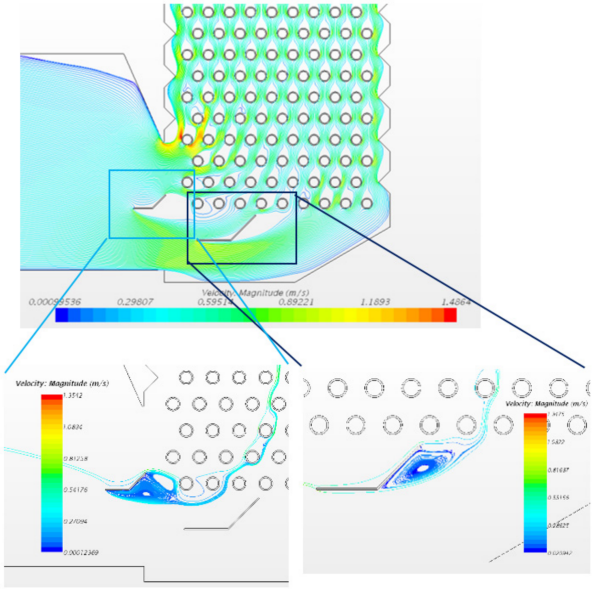

Figure 7. Streamlines inside an economizer with a conventional baffle installed.

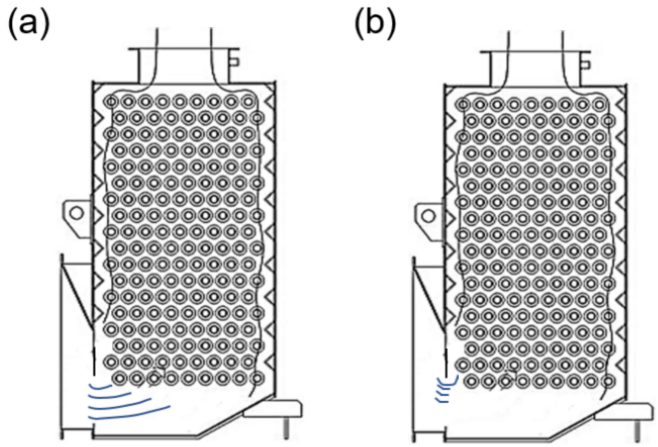

Figure 8. Two turning guide vane designs for heat and flow uniformity in the economizer: (**a**) TGV 1; (**b**) TGV 2.

As will be discussed in detail later, in Figure 2b, the existing baffle increased the pressure drop in the economizer by about 15%. In TGV 1, the possibility of causing an additional pressure drop was raised as four guide vanes, twice as many as before, were installed. In addition, [17] showed that it is advantageous to place the guide vane intervals intensively at locations where the flow rate is high. TGV 2 was designed to solve these problems and tried to minimize the pressure loss by arranging the guide vane only near the inlet in proportion to the mass flow rate at the economizer inlet.

Figure 9 shows the change in streamlines when TGVs 1 and 2 were installed compared to when there were no guide vanes. Compared to the conventional guide vane shown in Figure 5, it can be observed that the recirculation area was greatly reduced. TGV 1 removed most of the recirculation area, but there was still some remaining. TGV 2 showed streamlines with almost no dead zones by removing more of the recirculating flow region. To eliminate the recirculation flow, the innermost U-shaped guide vane in TGV 2 played a key role. The flow uniformity at the entrance of the duct was superior to that of TGV 2 in TGV 1, but the flow uniformity at the beginning of the tube bank was at a similar level.

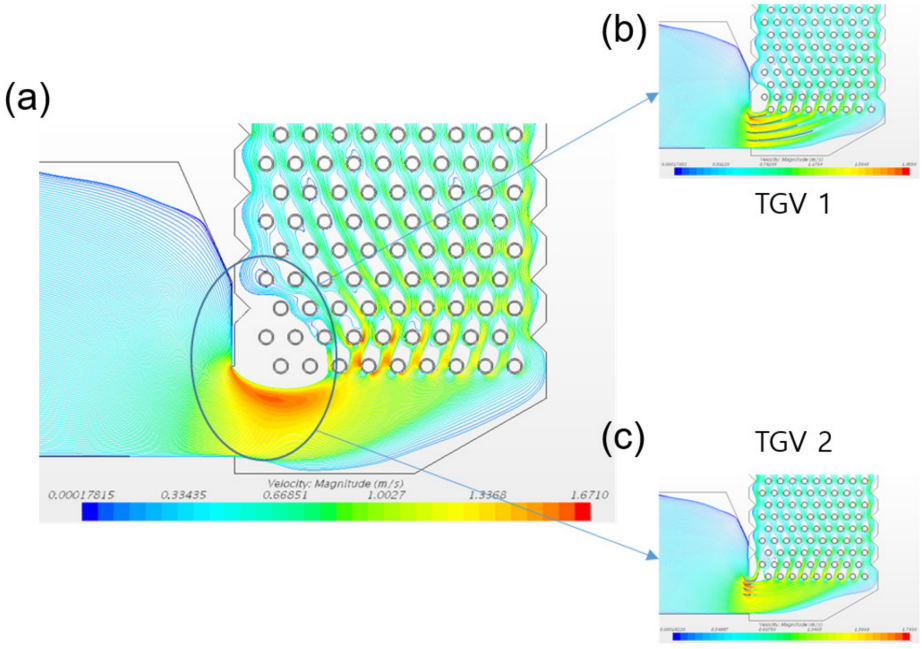

Figure 9. Streamlines inside an economizer: (**a**) without the baffle; (**b**) with TGV 1; (**c**) with TGV 2.

Figure 10 compares the temperature distribution of the four cases in which the simulation was performed. When there was no baffle or when the existing baffle was installed (Figure 10a,b), high-temperature areas (areas in red on the contour) were observed because heat transfer was not active in the inner part close to the connection duct. In addition, the high-temperature exhaust gas escaped without heating the water supply along the inside of the connecting duct and the connected economizer wall. In Figure 10a, the red area extends from the left wall to the economizer outlet. Most of the heat was transferred from the center of the economizer to the downstream side, resulting in a low-temperature region (bluish area on the contour).

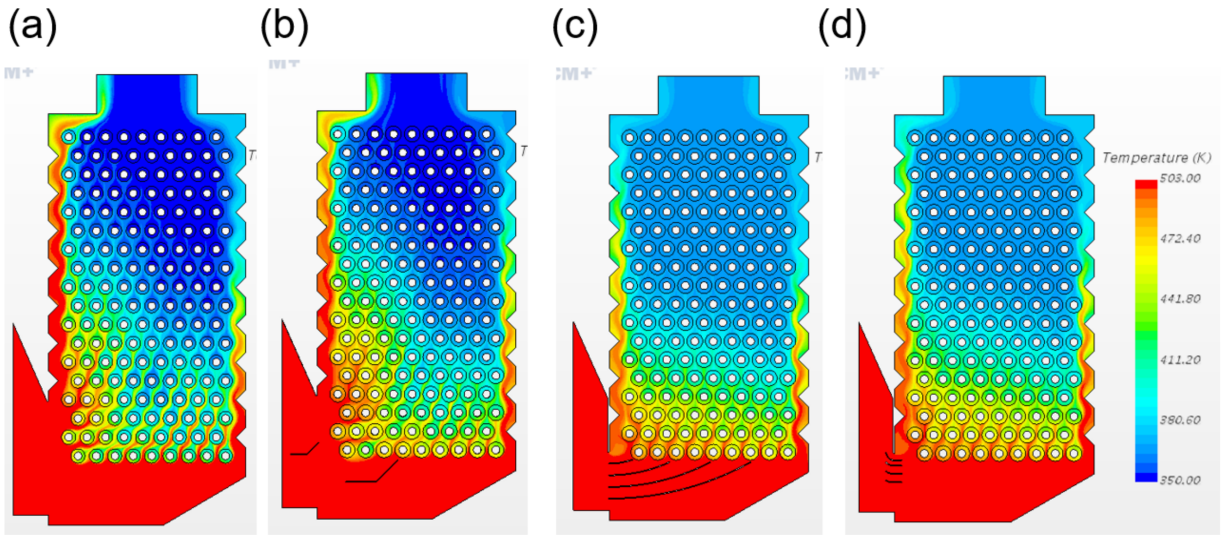

Figure 10. Temperature distributions inside the economizer: (**a**) without the baffle; (**b**) with the existing baffle; (**c**) with TGV 1; (**d**) with TGV 2.

Figure 10b, where the existing baffle was installed, shows a temperature distribution similar to Figure 10a, as these problems were still not resolved. When a TGV was installed (Figure 10c,d), the area of the hot zone at the economizer inlet was reduced. The effective heat transfer in the vicinity of the inner wall of the duct and the adjacent wall was similar to that of the vicinity in the outer wall. Heat transfer also actively occurred at the center; thus, the outlet temperature was much more uniform.

4. Discussion

Figure 11 compares the temperature distribution behind the fifth tube row. The CFD data for the original baffle (orange line) generally corresponded well with the experimental data (light green dots). Compared to the CFD results, it was difficult to accurately evaluate the temperature deviation with the four measurement points in one row of the experiment. The original baffle did not yield any significant improvement in temperature uniformity. As seen in the orange line of Figure 11, the temperature deviation shown in the blue line was reduced within x/W = 0.5, but the temperature deviation was not reduced significantly when x/W was over 0.5. TGVs 1 and 2 (gray and yellow lines) reduced the recirculation area and greatly increased the uniformity in the spanwise direction.

Figure 12 compares the temperature distribution at the downstream location, behind the tenth tube. Upon comparing the experimental (light green dots) and the CFD results (orange lines), it was found that the left area agreed well, but the right area CFD predicted the temperature slightly lower. Compared to the upstream location in Figure 11, the overall temperature became uniform. TGVs 1 and 2 (yellow and gray lines) greatly improved the temperature uniformity compared to the original baffle (orange line). There was no significant difference in temperature uniformity between TGVs 1 and 2.

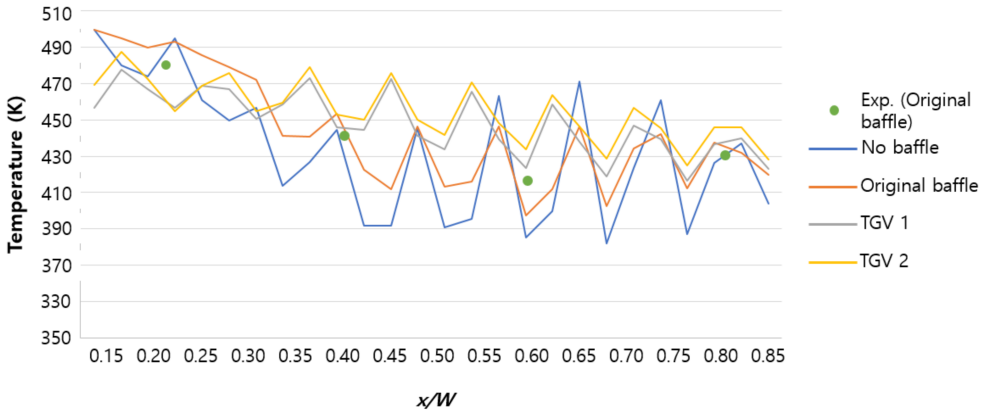

Figure 11. Spanwise temperature distribution behind the fifth tube row.

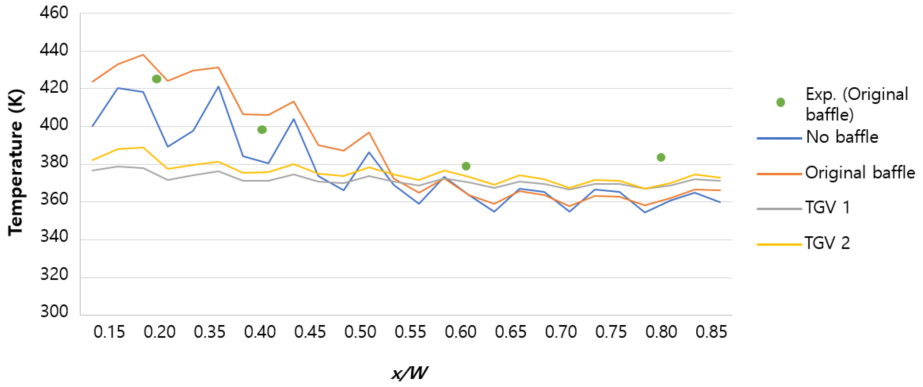

Figure 12. Spanwise temperature distribution behind the tenth tube row.

The temperature uniformity region was divided into three parts: near the inlet, in the middle, and near the outlet. The most uniform part was found in the middle (from rows 9 to 14). Being the research's objective, the inlet was most certainly the most non-uniform part. The area near the outlet part was slightly non-uniform, as the outlet acted as a contracting exit that converged the flue stream flow.

Figure 13 compares the temperature standard deviation in the width direction. In the upstream region, the standard deviation obtained from the CFD results was higher than that of the experimental ones. The temperature distributions compared in Figures 11 and 12 agreed relatively well with the experimental results, which could be attributed to a phenomenon caused by the lack of experimental data for obtaining standard deviations. The temperature deviation between the gray and yellow lines was much lower than that of the blue and orange lines. TGVs 1 and 2 greatly improved the temperature uniformity centered on the middle and upstream regions of the economizer.

Notably, on every design, the temperature on the front side was significantly higher than that on the backside of the economizer. This explains why the temperature uniformity for the odd-numbered row near the exit was lower than the even-numbered row, which was the effect of corbels installed on both sides to obtain a uniform flow rate in the staggered array of the tube banks.

Figure 14 compares the overall temperature standard deviation across all the economizers. The original baffle slightly improved the temperature uniformity near the economizer inlet; however, it deteriorated the temperature uniformity overall, increasing the spatial average temperature deviation by about 30%. However, TGVs 1 and 2 improved the uniformity and reduced the temperature deviation by more than 30%.

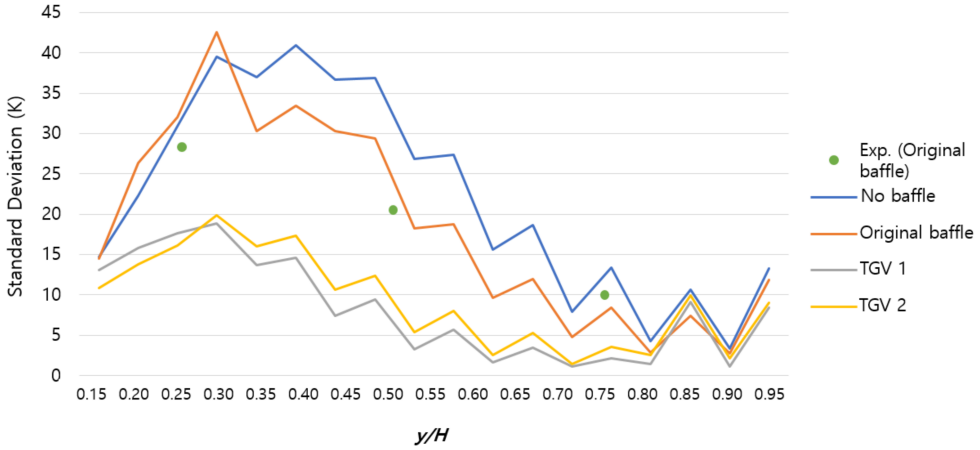

Figure 13. Streamwise variation of spanwise temperature uniformity.

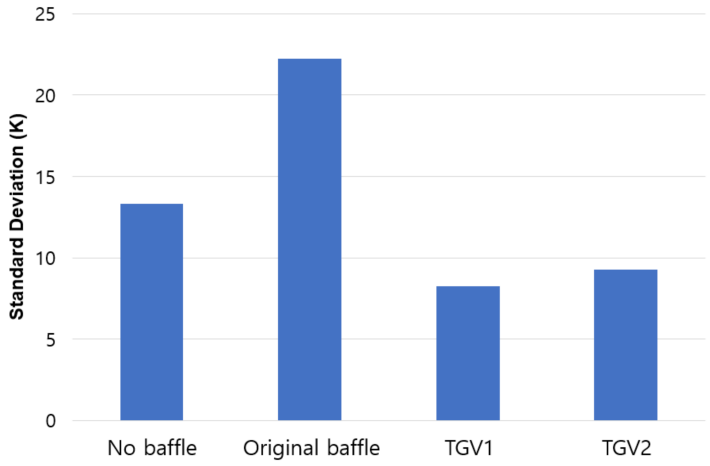

Figure 14. Streamwise-averaged spanwise temperature deviation.

The improvement of temperature uniformity was ultimately intended to promote heat transfer. In addition, baffles caused additional pressure loss, so heat transfer and pressure loss needed to be evaluated. There are several methods for evaluating performance by simultaneously considering heat transfer and pressure loss, but the economizer that performed CFD in this study was evaluated based on the volume goodness factor [27] because the purpose was to recover maximum heat from the exhaust gas.

Table 6 compares the heat transfer rate, pressure drop, and volume goodness factor of the four geometries for which CFD was performed. The original baffle increased the heat transfer rate by 14% and the pressure drop by 15% compared to when there was no baffle. Both TGVs 1 and 2 increased the heat transfer rate by 39% and the pressure drop by 40% and 37%, respectively. Compared to TGV 1, TGV 2 promoted heat transfer similarly, and the increase in pressure drop was slightly reduced.

Table 6. Volume goodness factor evaluation results.

Parameter	No Baffle	Original Baffle	TGV 1	TGV 2
Q (W)	143	163	199	199
ΔP (Pa)	37.9	43.5	53.0	51.8
$(Q/Q_s)/(\Delta P/\Delta P_s)^{1/3}$	1	1.09	1.24	1.26

In the spatial standard deviation shown in Figure 11, the original baffle was found to be unfavorable, but the volume goodness factor was greater than 1 (see Table 6). Although this

did not increase the overall temperature uniformity, it was determined that it enhanced heat transfer. TGV 2 showed temperature uniformity similar to that of TGV 1 and consequently yielded thermal performance. However, it did not reduce the pressure loss to the extent expected.

5. Conclusions

In this study, a TGV was installed in the upstream area of the economizer and connected vertically to a non-furnace boiler, and CFD was used to design and predict the performance of the TGV. For economical simulation, a convection condition was imposed on each tube row, and one pitch of a periodically installed fin was set as the computational domain. Star CCM+ was used for CFD. On the water side, a different heat transfer coefficient was applied to each row using a user-defined function by considering changes in physical properties. From the simulation results, it was found that the streamwise temperature drop was predicted similarly to the experimental and design data. By analyzing the streamlines obtained using CFD, two TGV designs were proposed. The first design placed guide vanes along the ducts to evenly divide the economizer inlet area and distribute the incoming flow evenly to the tube banks. The second design tried to reduce the pressure drop by arranging the guide vane according to the flow rate and installing the guide vane only near the economizer inlet. Both designs reduced the standard deviation of temperature by more than 30% and improved the volume goodness factor by 25%. TGV 2 yielded a heat transfer enhancement effect similar to that of TGV 1, but the expected pressure drop reduction effect was not significant.

Author Contributions: C.Q.A. carried out the simulations, analyzed the CFD data, and helped write the paper. J.A. supervised the research, analyzed the CFD data, and wrote the paper. All authors have read and agreed to the published version of the manuscript.

Funding: This work was supported by the Korea Institute of Energy Technology Evaluation and Planning (KETEP) and the Ministry of Trade, Industry and Energy (MOTIE) of the Republic of Korea (No. 20212020800070).

Institutional Review Board Statement: Not applicable.

Informed Consent Statement: Not applicable.

Data Availability Statement: Data are contained within this article.

Conflicts of Interest: The authors declare no conflict of interest.

References

1. Yalew, S.G.; van Vliet, M.T.; Gernaat, D.E.; Ludwig, F.; Miara, A.; Park, C.; van Vuuren, D.P. Impacts of climate change on energy systems in global and regional scenarios. *Nat. Energy* **2020**, *5*, 794–802. [CrossRef]
2. Olabi, A.G.; Abdelkareem, M.A. Renewable energy and climate change. *Renew. Sust. Energy Rev.* **2022**, *158*, 112111. [CrossRef]
3. Cozzi, L.; Gould, T.; Bouckart, S.; Crow, D.; Kim, T.Y.; Mcglade, C.; Wetzel, D. *World Energy Outlook*; International Energy Agency: Paris, France, 2020; pp. 1–461.
4. Echi, S.; Bouabidi, A.; Driss, Z.; Abid, M.S. CFD simulation and optimization of industrial boiler. *Energy* **2019**, *169*, 105–114. [CrossRef]
5. Ahn, J.; Kim, H.J. Combustion characteristics of 0.5 MW class oxy-fuel FGR (flue gas recirculation) boiler for CO_2 capture. *Energies* **2021**, *14*, 4333. [CrossRef]
6. Ahn, J.; Kim, J.J. Heat transfer characteristics of 0.5 t/h class non-furnace boiler with a metal fiber burner. *Trans. Korean Soc. Mech. Eng. B* **2011**, *35*, 215–220. [CrossRef]
7. Tang, W.; Feng, H.; Chen, L.; Xie, Z.; Shi, J. Constructal design for a boiler economizer. *Energy* **2021**, *223*, 120013. [CrossRef]
8. Li, J.; Wang, K.; Cheng, L. Experiment and optimization of a new kind once-through heat recovery steam generator (HRSG) based on analysis of exergy and economy. *Appl. Therm. Eng.* **2017**, *120*, 402–415. [CrossRef]
9. So, H.K.; Jo, T.H.; Lee, Y.H.; Koo, B.C.; Lee, D.H. Design optimization of HRSG inlet duct geometry for improving flow uniformity using meta-heuristic algorithm. *J. Mech. Sci. Technol.* **2018**, *32*, 947–958. [CrossRef]
10. Hanafizadeh, P.; Falahatkar, S.; Ahmadi, P.; Siahkalroudi, M.M. A novel method for inlet duct geometry improvement of heat recovery steam generators. *Appl. Therm. Eng.* **2015**, *89*, 125–133. [CrossRef]

11. Næss, E. Experimental investigation of heat transfer and pressure drop in serrated-fin tube bundles with staggered tube layouts. *Appl. Therm. Eng.* **2010**, *30*, 1531–1537. [CrossRef]
12. Beale, S.B.; Spalding, D.B. A numerical study of unsteady fluid flow in in-line and staggered tube banks. *J. Fluids Struct.* **1999**, *13*, 723–754. [CrossRef]
13. Muniandy, V.; Aziz, M.S.A.; Latip, H.F.M. Study on the improvement of heat recovery steam generator efficiency—A review. *J. Adv. Res. Fluid Mech. Therm. Sci.* **2022**, *94*, 89–98. [CrossRef]
14. Ameri, M.; Dorcheh, F.J. The CFD modeling of heat recovery steam generator inlet duct. *Int. J. Energy Eng.* **2013**, *3*, 74. [CrossRef]
15. Lee, B.E.; Kwon, S.B.; Lee, C.S. On the effect of swirl flow of gas turbine exhaust gas in an inlet duct of heat recovery steam generator. *J. Eng. Gas Turbines Power* **2002**, *124*, 496–502. [CrossRef]
16. Chabane, F.; Kherroubi, D.; Arif, A.; Moummi, N.; Brima, A. Influence of the rectangular baffle on heat transfer and pressure drop in the solar collector. *Energy Sources A Recovery Util. Environ. Eff.* **2020**, 1–17. [CrossRef]
17. Lee, S.Y.; Ahn, J.; Shin, S.W. Numerical optimization of temperature distribution in HRSG system using inlet guide vane. *J. Comput. Fluids Eng.* **2009**, *14*, 1–8.
18. Saravani, M.S.; Amano, R.S.; DiPasquale, N.J.; Halmo, J.W. Turning guide vane effect on internal cooling of two-passage channel with parallel ribs. *J. Energy Resour. Technol.* **2020**, *142*, 091303. [CrossRef]
19. Park, J.S.; Lee, D.M.; Lee, D.H.; Lee, S.; Kim, B.S.; Cho, H.H. Thermal performance in a rotating two-passage channel with various turning guide vanes. *J. Mech. Sci. Technol.* **2017**, *31*, 3581–3591. [CrossRef]
20. Valsala, R.R.; Son, S.W.; Suryan, A.; Kim, H.D. Study on reduction in pressure losses in pipe bends using guide vanes. *J. Vis.* **2019**, *22*, 795–807. [CrossRef]
21. Moon, M.A.; Kim, K.Y. Multi-objective optimization of a guide vane in the turning region of a rotating U-duct to enhance heat transfer performance. *Heat Mass Transf.* **2012**, *48*, 1941–1954. [CrossRef]
22. Ahn, J.; Hwang, S.S.; Kim, J.J.; Kang, S.B. Heat transfer characteristics of 2 t/h-class modular water-tube-type boiler. *Trans. Korean Soc. Mech. Eng. B* **2012**, *36*, 1127–1133. [CrossRef]
23. Incropera, F.P.; DeWitt, D.P.; Bergman, T.L.; Lavine, A.S. *Principles of Heat and Mass Transfer*; John Wiley & Sons: Hoboken, NJ, USA, 2017.
24. Winterton, R. Where did the Dittus and Boelter equation come from? *Int. J. Heat Mass Transfer* **1998**, *41*, 809–810. [CrossRef]
25. Kays, W.M.; London, A.L. *Compact Heat Exchangers*; Krieger Publishing Company: New York, NY, USA, 1984.
26. Lee, D.; Ahn, J.; Shin, S. Uneven longitudinal pitch effect on tube bank heat transfer in cross flow. *Appl. Therm. Eng.* **2013**, *51*, 937–947. [CrossRef]
27. Webb, R.L. Performance evaluation criteria for use of enhanced heat transfer surfaces in heat exchanger design. *Int. J. Heat Mass Transf.* **1981**, *24*, 715–726. [CrossRef]